New Journal of Physics
The open access journal at the forefront of physics

Deutsche Physikalische Gesellschaft DPG IOP Institute of Physics

PAPER • OPEN ACCESS

Impact of particle charge and electrorheology-effects on dust-acoustic waves in low pressure complex plasma under microgravity

To cite this article: L Wimmer *et al* 2025 *New J. Phys.* **27** 033001

View the article online for updates and enhancements.

You may also like

- Slow post-fire carbon balance recovery despite increased net uptake rates in Alaskan tundra
Jacqueline K Y Hung, Kyle A Arndt, Patrick Murphy et al.
- Introducing the DREAMS Project: DaRk mattEr and Astrophysics with Machine Learning and Simulations
Jonah C. Rose, Paul Torrey, Francisco Villaescusa-Navarro et al.
- Phonon effects, impact ionization and power conversion in Mott photovoltaic systems
Paolo Gazzaneo and Enrico Arrigoni

4-CHANNEL CONFIGURABLE OPEN RF ENGINE FOR QUANTUM EXPERIMENTS

LUGUS
Developed by Instrumentation Technologies

High bandwith arbitraty waveform generator (AWG)
Up to 1.25 GSPS

Open & programmable
Full access to FPGA implementation and firmware

Compatible with control frameworks
LabScript, ARTIQ, etc.

High power outputs
Up to 36 dBm

High-bandwidth feedback control
Open or closed-loop operation, Feedback bandwidth up to 125 MSPS

This content was downloaded from IP address 134.176.174.210 on 23/10/2026 at 08:07

IOP Publishing New J. Phys. 27 (2025) 033001 https://doi.org/10.1088/1367-2630/adb876

New Journal of Physics
The open access journal at the forefront of physics

Deutsche Physikalische Gesellschaft DPG
IOP Institute of Physics

Published in partnership with: Deutsche Physikalische Gesellschaft and the Institute of Physics



OPEN ACCESS

RECEIVED
19 November 2024

REVISED
14 February 2025

ACCEPTED FOR PUBLICATION
20 February 2025

PUBLISHED
28 February 2025

Original Content from this work may be used under the terms of the Creative Commons Attribution 4.0 licence.

Any further distribution of this work must maintain attribution to the author(s) and the title of the work, journal citation and DOI.



PAPER

Impact of particle charge and electrorheology-effects on dust-acoustic waves in low pressure complex plasma under microgravity

L Wimmer[1,*], N Dormagen[1,2], M Klein[1,2], M Kretschmer[1,2], A M Lipaev[3], M Schwarz[2], A D Usachev[3], O F Petrov[3], A V Zobnin[3] and M H Thoma[1]

[1] Institute of Experimental Physics I, Justus-Liebig University, 35392 Gießen, Germany
[2] NanoP, THM University of Applied Sciences, D 35390 Giessen, Germany
[3] Joint Institute for High Temperatures, Russian Academy of Sciences, 125412 Moscow, Russia
[*] Author to whom any correspondence should be addressed.

E-mail: lukas.wimmer@epx1.physik.uni-giessen.de

Keywords: complex plasma, two-stream instability, electrorheology, microgravity

Abstract

This study investigates the influence of particle charge and electrorheological (ER) effects on microparticle dynamics and dust-acoustic wave propagation in low-pressure complex plasmas under microgravity conditions. Experiments were conducted using PK-4 during parabolic flights and onboard the International Space Station to analyze dust particle behavior in direct current (DC) and DC polarity switching discharge plasma. Key findings reveal that variations in particle charge potential and ER effects significantly affect particle dynamics, especially at different gas pressures. Specifically, we validated a dimensionless charge potential of $z = 0.34 \pm 0.17$ in a DC neon plasma discharge, noting a rapid increase in this potential at pressures below 15 Pa. Furthermore, we observed a reduction in charge of up to 50% due to quadrupole effects induced by polarity switching. These results provide critical insights into plasma behavior in microgravity and the role of external electric fields in particle interactions.

1. Introduction

Plasma, commonly recognized as the fourth fundamental state of matter, exhibits unique electrical conductivity properties. It typically forms when gas molecules are ionized under conditions such as high temperatures, electrical discharges, or exposure to other ionizing sources of energy. This process results in the breakdown of the gas into a collection of freely moving charged particles, including electrons and ions. The ionized state sets plasma apart from the classical states of matter—solid, liquid, and gas. It is a key phenomenon in various technological applications, including but not limited to semiconductor processing, environmental monitoring, medical technology, and the generation of energy through controlled nuclear fusion. Significantly, plasma constitutes roughly 99% of the visible Universe, highlighting its importance in both earth-bound and cosmic contexts [1].

Within the field of plasma physics, complex plasmas containing micron-sized dust particles present intriguing properties and behaviors. One of the key phenomena observed in such environments is the dust-acoustic wave (DAW), a low-frequency and long-wavelength oscillation involving the dust particles themselves [2]. These waves are particularly interesting for study under microgravity conditions, such as those provided by space-based experiments, where gravitational effects are minimized, allowing for clearer observation of underlying plasma behaviors [3].

This study focuses on the impact of particle charge and electrorheology (ER) on the speed of DAWs in direct current (DC) discharge plasma under microgravity conditions. Electrorheology refers to the changes in the rheological properties of a fluid due to the presence of an alternating-current (AC) electric field. In the context of plasma, this phenomenon can significantly alter the interactions between charged dust particles, influencing both the characteristics of individual particles and DAWs.

© 2025 The Author(s). Published by IOP Publishing Ltd on behalf of the Institute of Physics and Deutsche Physikalische Gesellschaft

Previous research has extensively explored the generation and propagation of DAWs in various plasma environments, including DC glow discharges and radio-frequency (RF) discharges [4, 5]. These studies have provided valuable insights into the mechanisms driving these waves and the conditions under which they occur. However, the influence of electrorheological (ER) effects, particularly under microgravity, remains an area requiring further investigation.

In microgravity, dust particles in plasma can achieve configurations and dynamics distinct from those observed under Earth's gravity. This environment facilitates the study of DAWs with minimal external perturbations, providing a clearer understanding of the fundamental processes involved. Additionally, the unique properties of ER fluids, where particles align into structured formations under an electric field, provide new insights into DAW dynamics [6, 7].

This paper aims to examine the phase speed of DAWs and the trajectories of dust particles in a low-pressure DC discharge plasma under microgravity. By analyzing these aspects, we aim to enhance the understanding of how particle charge and electrorheology influence wave propagation. The findings are expected to contribute to broader applications in space physics, materials science, and astrophysics, where understanding plasma dynamics at a granular level is crucial.

The effective interparticle interaction is governed by the time-averaged wake potential. Within the framework of the linear response formalism, this interaction becomes rigorously reciprocal (Hamiltonian). Consequently, one can directly apply the principles of statistical physics to describe the dynamics of ER plasmas. This theoretical understanding is crucial for predicting and controlling the behavior of DAWs under the influence of ER effects [8].

The organization of this paper is as follows: section 2 describes the experimental setup and procedures used to generate and observe DAWs. Section 3 discusses the key parameters and theoretical models applied in the analysis of experimental results. Finally, section 4 summarizes the key findings and implications of the study, providing insights into the complex interactions within plasmas influenced by ER effects under microgravity conditions.

2. Experimental setup and procedure

The investigation of dust acoustic waves (DAWs) was conducted using the PK-4 setup during parabolic flight (PFC) DLR campaign 42 and onboard the International Space Station (ISS) during campaign 15. Both plasma chambers, illustrated in figure 1, are identical, enabling a controlled study of specific phenomena under various conditions [9, 10].

In both setups, plasma is generated within a Π-shaped glass tube (inner diameter $2R = 3\,\mathrm{cm}$) filled with neon gas at a pressure range of $p = 15 - 40$ Pascal (Pa). A discharge current of $I_{\mathrm{DC}} = 0.5\,\mathrm{mA}$ is used to create a DC discharge in the 86 cm long tube, providing a suitable environment to analyze multi-particle phenomena using a green laser illumination system and a digital camera [10].

For the parabolic flight setup, observations were captured using a CMOS camera with a 4-megapixel resolution and a pixel size of $11.8\,\mu\mathrm{m}$. This setup resulted in a field of view (FOV) of $24 \times 24\ \mathrm{mm}^2$, with recordings conducted at a frame rate of 80 fps, as shown in the images in figure 1, right panel, for 40 and 15 Pascal. Due to the limited operation time in microgravity (approximately 22 s per maneuver), the procedure had to be both rapid and efficient.

In contrast, the ISS setup utilized cameras with a resolution of $14.2\,\mu\mathrm{m}$ and a smaller FOV of $23 \times 17\ \mathrm{mm}^2$, operating at 35 fps. The FOV height was adjusted to half in order to improve readout time and boost the frame rate to 60 fps. Additionally, the ISS setup allowed for the confinement of the particle cloud using RF coils, enabling detailed scans through the cloud to examine particle density and ensure a fully extended cloud with a high particle population [10].

The experimental procedure involved injecting a cloud of microparticles into the plasma chamber. Each microparticle had a diameter of $2a = 3.4\ \mu\mathrm{m}$, was composed of melamine-formaldehyde (MF) material with a density $\rho_{\mathrm{d}} = 1.5\,\mathrm{g\,cm^{-3}}$, and a mass of $m_{\mathrm{d}} = 3.24 \cdot 10^{-11}\,\mathrm{g}$. These particles acquired a charge of approximately 1500 e by collecting electrons and ions from the plasma. The longitudinal electric field of about $2\,\mathrm{V\,cm^{-1}}$ in the positive column of the discharge caused the particles to drift through the plasma chamber [10].

During the experiment, the particle cloud was transported bidirectionally through the tube by systematically modulating the effective electric field strength (E_{eff}) through polarity switching. Specifically, the duty cycle of the polarity-switching electric field was adjusted to directly control the E_{eff}. A 50% duty cycle results in an effectively neutral field ($E_{\mathrm{eff}} = 0\%$), while reducing the duty cycle proportionally increases the magnitude of E_{eff}. This method allowed us to observe the behavior of self-excited DAWs, which occur at pressures below 50 Pa. The particle cloud exhibited stable drifting at a constant velocity, with counteracting ions resulting in a two-stream instability that generated DAWs [7, 10].

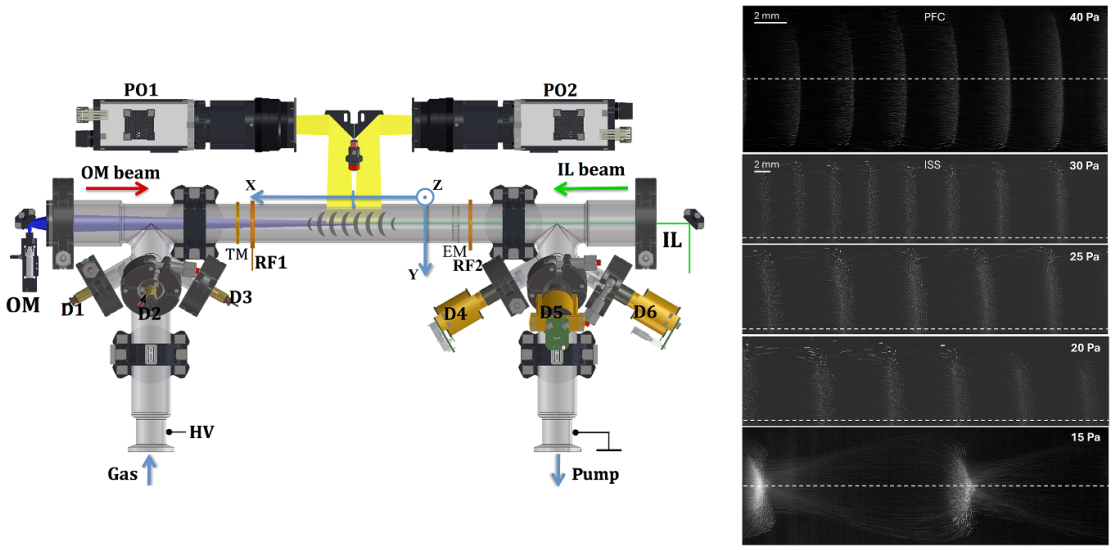


Figure 1. A schematic depiction is presented in the left panel, illustrating the experimental setup and procedure employed. © [2016] IEEE. Reprinted, with permission, from [12]. The process involved injecting a densely populated particle cloud into the chamber, which then traversed through the chamber. Key components and manipulation tools are identified, including the illumination laser (IL) and optical manipulation laser (OM). Additionally, the setup includes radio-frequency (RF) coils, electromagnetic (EM) manipulators, and thermal manipulators (TM). Particle injection is achieved using dispensers D1–D6, and the observed phenomena are captured by the particle observation cameras (PO). The right panel displays example images of self-excited Dust Acoustic Waves (DAWs) at different gas pressures, captured during the ISS and PF campaigns. In particular, high-contrast images of these waves are presented for gas pressures of 15 Pa and 40 Pa from the PF campaign, and 20 Pa to 30 Pa from the ISS campaign. A dashed line marks the center of the plasma chamber in each image.

In the ISS setup, the procedure included trapping of the particle cloud using RF-coils, providing sufficient time to experiment under microgravity conditions. The confined particle cloud expanded to the plasma sheath with enough density to excite DAWs. With this it was possible to systematically scan the particle cloud and examine the particle cloud density for every configuration, see analysis section. By controlling the current and pressure, we could adjust the impact of the plasma on the particle cloud, altering their behavior.

The experimental procedure concluded with a series of runs where the particle cloud was sent back and forth through the tube. During these runs, the effective electric field in the chamber was systematically reduced by adjusting the DC polarity switching (DC-PS) duty cycle. When an alternating electric field is applied to the complex plasma at a frequency much higher than the microparticle plasma frequency ($f_{\mathrm{pd}} =$ 10–100 z) and much lower than the ion plasma frequency (about 10 MHz) [11], the microparticles experience an averaged electric field that depends on the duty cycle of the polarity switching. This manipulation of the electric field influenced the behavior of the DAWs and provided valuable insights into the ER effects impacting the multi-particle system. The polarity switching was carried out at a frequency of 500 Hz, ensuring precise control over the microparticle dynamics and the resultant wave phenomena.

3. Theoretical methodes

In this section, we outline the theoretical framework employed for the analysis of individual particles and DAWs. We begin by detailing the particle charge potential and its behavior in large particle clouds. Subsequently, we present the force equations governing the trajectories of individual particles. A key aspect of our methodology involves describing DAWs through the dispersion relation. Finally, we address ER effects, establishing the theoretical foundation for the subsequent discussion and analysis.

3.1. Charge and charge depletion

The methodology for estimating the charge on microparticles in a complex plasma is outlined here, along with an analysis of how the Havnes Parameter influences the overall charge of multiparticle clouds in the plasma environment.

The charge of individual particles, denoted as Z_{d}, in the bulk of the discharge is estimated using the model presented in Antonova *et al* [13]. The charge formula, expressed as a function of the particle's potential, is given by:

$$Z_{\mathrm{d}} = (4\pi\varepsilon_0 k_{\mathrm{B}})\,\frac{zaT_{\mathrm{e}}}{e^2}; \qquad z = 0.3 \pm 0.1. \tag{1}$$

Here, z represents the reduced charge, which relates to the potential of a microparticle within a neon complex plasma, taking into account its radius a_p, with T_e denoting the electron temperature. This potential was experimentally estimated as indicated in equation (1) and is used as basic [13].

The Havnes parameter, denoted as P_H, plays a significant role in modifying the bulk particle charge due to interactions within a densely packed grain environment [14, 15]. It is defined as the ratio of the charge residing on the dust component to that on the electron component, calculated by the following formula:

$$P_H = \frac{4\pi\epsilon_0 a}{e}\left(k_B T_e/e\right)\left(n_d/n_i\right) \tag{2}$$

where n_d and n_i are the grain and ion number densities, respectively and k_B denotes the Boltzmann constant [14]. This parameter effectively captures the interaction effects among closely packed grains, which contribute to the quasineutrality condition, $n_i = n_e + Z_d n_d$, making the ion density larger than the electron density. This interaction increases the ratio of ion-to-electron flux, thereby reducing the absolute magnitude of the grain charge compared to an isolated grain scenario [14].

The estimation of electron and ion fluxes via the orbital motion limited (OML) approach, together with the quasineutrality condition, leads to a dimensionless representation:

$$\sqrt{\tau}\exp\left(-z\right) = \sqrt{\frac{m_e}{m_i}}\left(1+z\tau\right)\left(1+P_H\right) \tag{3}$$

where m_e and m_i are the electron and ion masses, respectively. This equation incorporates the effects of particle density and the Havnes parameter, with $\tau = T_e/T_i$, where T_i is the ion temperature, on the overall charge dynamics within the plasma, providing a comprehensive perspective on how microscale interactions influence macroscale plasma characteristics.

The application of basic OML theory involves certain limitations that warrant discussion. Specifically, this theory's limitations are partially addressed by incorporating charge modification due to closely packed dust particles, as accounted for by the Havnes parameter. However, our model omits an additional critical effect: ion collisions with neutral particles, which diminish the current flow into the microparticles, subsequently reducing the particle charge number, z [5, 16]. It is essential to emphasize that our results represent the upper boundary for particle charge, as they do not account for the potential charge reduction caused by ion-neutral collisions.

3.2. Force balance

The velocity of particles within a stable flow regime is dictated by the equilibrium of various forces acting upon them. These forces include the electric force, $F_E = -Z_d eE$, the neutral drag force, $F_n = -\delta\frac{4}{3}\pi a^2 m_n \nu_{th,n} n_n \nu_d$, and the ion drag force, $F_{id} = m_d\nu_{di}(u_i - v_d) \approx m_d\nu_{di}v_d$ [17]. Within the observed conditions, the electron drag force is significantly smaller, by almost two orders of magnitude, than the ion drag force, thus, it is neglected in our theoretical assumptions. This disparity arises due to the substantial electron-to-ion temperature ratio $\tau = T_e/T_i$ [18]. In the expressions for the neutral drag force, $\delta = 1.4$ represents a factor that characterizes the interactions between gas molecules and spherical particles, accounting for the resultant velocity distribution of particles reflected from the surface [19]. Moreover, m_n represents the mass of a neutral gas atom, $\nu_{th,n}$ denotes the thermal velocity of the neutrals, and n_n their number density. In the general description of the ion drag force, u_i denotes the ion drift velocities, and ν_{di} correspond to the effective momentum transfer frequencies for dust-ion collisions. The measured velocity of a microparticle with mass m_d and radius a is represented by v_d. Finally, the addressed forces are collected in a balance equation given by:

$$F_n + F_E + F_{id} = 0. \tag{4}$$

However, the ion drag force is complex in many ways, especially the interaction between microparticles and ions. For the momentum transfer during dust-ion collisions, we adopt an established heuristic expression suitable for our experimental parameter space [17]:

$$\delta\frac{4}{3}\pi a^2 m_n \nu_{th,n} n_n \nu_d = -Z_d eE + \left(8\sqrt{2\pi/3}\right)a^2 n_i m_i \nu_{Ti} u\cdot\Phi_\Lambda, \tag{5}$$

$$\Phi_\Lambda = \left[1 + \frac{\beta_T}{2}\frac{\lambda_D}{a} + \frac{\beta_T^2}{4}\frac{\lambda_D^2}{a^2}\Lambda\right], \tag{6}$$

where m_i is the ion mass, $v_{Ti} = \sqrt{T_\mathrm{i}/m_\mathrm{i}}$ represents the ion thermal velocity and,

$$\Lambda = 2\int_0^\infty \left[\exp(-x)\ln\left(\frac{2x+\beta_T}{2ax/\lambda_\mathrm{D}+\beta_T}\right)\right]\mathrm{d}x, \tag{7}$$

is the modified Coulomb logarithm, integrated over the Maxwellian velocity distribution function for ions, with the thermal scattering parameter $\beta_T = Ze^2/T_\mathrm{i}\lambda_\mathrm{D}$ and Debye length λ_D representing the effective screening length [18]. The ion drift velocity and the electric field are related via the ion mobility coefficient, $u = \mu E = M \cdot v_{Ti}$. The ion flow, caused by the electric field, naturally results in the momentum transfer from the ions drifting relative to the particle component. The modified Frost approximation of the mach number, M, is given by [20]:

$$M = A \cdot \left[1 + \left(B \cdot \frac{E}{N}\right)^C\right]^{-1/2C} \frac{E}{N}. \tag{8}$$

Here, E/N represents the ratio of electric field strength to the neutral gas number density, expressed in Townsend units ($1\,\mathrm{Td} = 10^{-17}\,\mathrm{V}\cdot\mathrm{cm}^2$), and coefficients $A = 0.0354\,[\mathrm{Td}^{-1}]$, $B = 0.0118\,[\mathrm{Td}^{-1}]$, and $C = 1.181\,[\mathrm{Td}^{-1}]$.

An additional adjustment is required when operating in low-pressure complex plasmas, as it affects the ion temperature, T_i. Typically, the ion temperature is assumed to be equal to that of neutral atoms, approximately 300 K. However, under low-pressure conditions, the ion temperature increases due to heating in the ambipolar diffusion field, E, resulting in a temperature corresponding to two-thirds of the mean energy of ions drifting in the electric field. Consequently, the interparticle distance increases, which directly impacts the ion temperature, as described in [21, 22]:

$$\tilde{T}_\mathrm{i} = \frac{2}{9} l_\mathrm{i} e E. \tag{9}$$

This adjustment is critical for accurately modeling the behavior of ions in low-pressure plasmas involving the ion mean free path l_i and electric field potential E.

3.3. Linear dispersion relation

The dispersion relation is a valuable tool to assess the experimental data and results for DAWs in complex plasmas, particularly in its linear form. The derivation of the dispersion relation for DAWs takes into account three charged species: electrons, ions, and dust particles, all of which are assumed to be undergoing linear motion along the x-axis. However, following the standard textbook procedure and using the quasi-neutrality condition, $n_\mathrm{i} = n_\mathrm{e} + Z_\mathrm{d} n_d$, the dispersion relation is simplified by assuming cold dust ($T_\mathrm{d} = 0$) and hot electrons ($T_\mathrm{i} << T_\mathrm{e}$) to [15],

$$\omega^2 + i\beta_\mathrm{d}\omega = \frac{\omega_\mathrm{pd}^2 k^2 \lambda_\mathrm{D,i}^2}{1 + k^2\lambda_\mathrm{D,i}^2}, \tag{10}$$

with the wave and dust plasma frequency ω, ω_pd, the dust-neutral friction coefficient β_d, the wave vector k and the ion Debye length λ_Di. At this point, we have to take a closer look at β_d, characterizing the damping rate of the linear system [15],

$$\beta_\mathrm{d} = \frac{8\cdot\delta}{\pi} \cdot \frac{p}{a\rho_\mathrm{d} v_\mathrm{th,n}}, \tag{11}$$

with the Epstein coefficient δ, pressure p and MF-density ρ_d [19]. Additionally, the neutral thermal velocity, denoted as $v_\mathrm{th,n}$ and defined by $v_\mathrm{th,n} = \sqrt{T_\mathrm{n}/m_\mathrm{n}}$, is fixed at 320 m s^{-1}, where m_n represents the neutral mass. All important quantities are given in table 1. A quantitative analysis of the interplay between the dust-friction parameter and the plasma-dust interaction frequency indicates minimal effects [15]. This result suggests a negligible impact on wave damping, as the dust friction coefficient β_d ranges from $0.52\cdot\omega_\mathrm{pd}$ to $0.13\cdot\omega_\mathrm{pd}$. A direct comparison with the measured wave frequency and its influence maybe problematic, as the actual phase frequency deviates from that relative to the background gas. However, we aim for a straightforward discussion using a linear approach. Therefore, we assume zero damping in the subsequent sections of this

paper. Additionally, taking into account small wave numbers where $k^2\lambda_{\mathrm{Di}}^2 \ll 1$, a condition met in all observed cases, the dust-acoustic phase speed C_{DAW} is determined by

$$C_{\mathrm{DAW}} = \omega_{\mathrm{pd}}\lambda_{\mathrm{Di}} = \sqrt{\frac{k_{\mathrm{B}}T_{\mathrm{i}}}{m_{\mathrm{d}}} \cdot \frac{n_{\mathrm{d}}}{n_{\mathrm{i}}} \cdot Z_{\mathrm{d}}^2}, \tag{12}$$

with the ion temperature T_{i} and the mass of a single micro-particle m_{d}.

3.4. ER effect

This section addresses the analytic aspects of the ER effects influencing the speed of micro particles and DAWs in complex plasmas. The primary focus is on the particle charge potential and the interaction dynamics shaped by the external electric field.

In a complex plasma, the effective radius of the polarizable cloud attached to a microparticle, typically defined by the ion screening length, is typically a few orders of magnitude larger than the particle size itself, $2 \cdot a/\lambda_{\mathrm{D}} \ll 1$. In the absence of an external electric field, this polarizable cloud maintains a spherical shape, known as the Debye sphere. However, upon the application of an external field, the cloud loses its symmetry and assumes a more complicated, asymmetric shape. The center of this asymmetric cloud, termed the ion wake, is displaced downstream relative to the grain along the direction of the field-induced ion drift. This leads to a nonreciprocal (non-Hamiltonian) interaction between charged grains. Such nonreciprocity arises because the wakes, which are essentially extensions of the surrounding plasma, act as a tenuous third body in the interaction dynamics. Nonreciprocity could be eliminated only if the wake potential were an even function of coordinates, i.e. $\Phi(r) = \Phi(-r)$. A method to achieve a reciprocal wake potential involves applying an AC or DC-PS field. The frequency of this field should be significantly lower than the ion plasma frequency (typically $\sim 10^7\,\mathrm{s}^{-1}$) yet substantially higher than the dust plasma frequency (typically $\sim 10^2\,\mathrm{s}^{-1}$). Under these conditions, the ions respond almost instantaneously to the alternating field, while the microparticles remain essentially unresponsive. The effective interparticle interaction is then governed by the time-averaged wake potential.

Within the framework of the linear response formalism, this interaction becomes rigorously reciprocal (Hamiltonian). Consequently, we can directly apply the principles of statistical physics to describe the dynamics of ER plasmas with $\Phi \approx \Phi_Y + \Phi_Q$, where Φ_Y represents the ideal Yukawa-Potential and:

$$\Phi_Q(r,\Theta) \simeq Z_{\mathrm{d}}\left[-\left(2-\frac{\pi}{2}\right)\cdot\frac{M^2\lambda_{\mathrm{D}}^2}{r^3}\left(3\cos^2\Theta - 1\right)\right] \tag{13}$$

represents the quadrupole term [8, 23], with relative microparticle distance r and particle charge Z_{d}. This interplay results in measurable side effects, including the formation of string-like structures composed of microparticles. Strings are defined as electrorheologically connected particles that appear in a chain-like structure. They are identified by analyzing the angle between neighboring particles at a constant distance, which determines the likelihood of string formation [24]. Evidence suggests that the likelihood of string formation between microparticles increases in the presence of ER effects [6]. Furthermore, the influence of string formation on DAWs has been quantified [7].

4. Results and analysis

In this section, we present the evaluation of the charge and collective behavior of a microparticle ensemble under varying effective electric field strengths, E_{eff}. As an initial step, table 1 provides an overview of essential physical parameters, excluding the final results. Parameters marked with a star ($\star$) were measured in the absence of microparticles using a Langmuir probe and subsequently adjusted to reflect the experimental conditions [10].

The particle number density, n_{d}, is determined using image reconstruction techniques incorporating machine learning methods [25]. In this approach, particle motion is arrested by inducing an electric field through an RF coil, which applies an alternating current (AC) field of 300 mW at a frequency of 81.36 MHz. This leads to the formation of a crystalline particle structure, characterized by a central void in the confined particle cloud. For a detailed description of the procedure, refer to section 2. The three-dimensional particle density is estimated using the Wigner–Seitz cell approximation, based on particle tracking data to determine the pair correlation function. The mean radius, r_0, is identified from the first peak of the radial distribution function, and the Wigner–Seitz radius is subsequently calculated as $a_w = r_0/\rho$, where $\rho = 1.79 \pm 0.07$ represents the assumed packing density [26]. This provides an estimate of the particle number density with a maximum uncertainty of $\pm 12\%$, assuming isotropic cloud symmetry [23, 27]. However, due to the symmetric distribution of particles induced by the RF coil, the reference particle density was determined as

Table 1. Summary of system parameters and performance metrics. Quantities marked by ($\star$) are measured in the absence of microparticles, taken from [10], while others are deduced from theoretical considerations. Detailed descriptions and applications are provided in the text.

Parameter	15 Pa	20 Pa	25 Pa	30 Pa	40 Pa
$E^\star$ [V m^{-1}]	−249	−248	−248	−247	−246
$n_\mathrm{d} \cdot 10^{11}$ [m^{-3}]	0.65	1.50	1.90	2.30	2.50
$n_\mathrm{i} \cdot 10^{14}$ [m^{-3}]	3.66	2.86	2.84	2.86	2.73
$n_\mathrm{e}^\star \cdot 10^{14}$ [m^{-3}]	0.85	0.92	0.99	1.06	1.20
$n_0 \cdot 10^{21}$ [m^{-3}]	3.75	4.99	6.24	7.49	9.99
$T_\mathrm{e}^\star$ [eV]	10.08	9.59	9.20	8.91	8.56
T_i [eV]	0.0448	0.0411	0.0388	0.0373	0.0355
$l_\mathrm{i} \cdot 10^{-4}$ [m]	2.67	2.00	1.60	1.33	1.00
λ_D [μm]	82	89	87	85	84
M	1.68	1.34	1.10	0.94	0.72
u_i [m s^{-1}]	647.5	484.7	387.0	321.9	240.5
P_H	1.80	2.17	2.13	2.08	2.14
ω_pd [1/s]	796	549	522	509	433
β_d [1/s]	98.14	130.86	163.57	196.28	261.71

$n_\mathrm{d} = 2 \cdot 10^{11}$ [m^{-3}] for all pressures. A more detailed analysis reveals stronger deviations, which will be discussed in the following sections.

The electron number density, n_e, and electron temperature, T_e, are measured in the absence of microparticles [10]. Conversely, the ion number density, n_i, and ion temperature, T_i, are inferred based on the quasineutrality condition, $n_\mathrm{i} = n_\mathrm{e} + Z_\mathrm{d} n_\mathrm{d}$, and the ion mean free path, l_i, using equation (9).

The ion mean free path is determined by the neutral gas density and calculated using the ideal gas equation: $l_\mathrm{i} = 1/(n_\mathrm{n}\sigma_\mathrm{in}) \approx T_\mathrm{n}/p\sigma_\mathrm{in}$, where $\sigma_\mathrm{in} = 10^{-18}\,\mathrm{m}^2$ represents the ion-neutral cross-section of neon plasma [18].

Other significant parameters, such as the ion velocity u_i, are derived using the Frost formula, equation (8), which relates the Mach number of the ion species to the system parameters. The ion velocity's direct proportionality to the electric field forms the basis of the analysis presented in section 4.2.

4.1. Charge

The initial findings from the measurements performed during the ISS campaign (blue) and the parabolic flight campaign (red) are presented in figure 2. We observe the expected trend of the measured data, showing a higher particle velocity, v_group, and wave phase velocity, C_DAW, at low pressure, reducing to higher pressure values within the observed range. Notably, the data collected during the PFC are slightly higher. This discrepancy may stem from procedural differences between the flight and ISS campaigns, which could influence the microparticle trajectories and their interaction with the radial electric field before reaching the FOV, leading to an increase in particle charge an effect likely more pronounced at lower pressures [22]. However, it is important to note that a direct comparison assumes equivalency in the electric field potential across both the PFC and ISS setups, which cannot be guaranteed and may also account for observed deviations.

The figures also show the theoretical prediction for each observation. The combination of the two theoretical models allows us to estimate the charge potential by solving equations (5) and (12) numerically. This also involves solving equation (3) to account for charge depletion caused by closely packed particles, as predicted by the Havnes parameter P. The Havnes parameter is plotted in the top panel and the resulting depleted charge potential z_depl in the bottom panel, on the second axis of figure 2. By fitting these models, we obtain a final charge estimation, with error estimates derived from fitting the solutions to the measured maximum combined uncertainties. This method has been established and used in various prior publications [7, 22, 26].

Table 2 provides a summary of the key findings. Figure 3, presents the final results for z (z_depleted) and compares them with findings from previous studies. For this comparison, the charge potential is plotted against a dimensionless parameter, defined as the ratio of the ion Debye length to the ion mean free path. Our results show a trend consistent with those reported in earlier publications, indicating that the model accurately describes our experimental observations. However, there is a discrepancy in the absolute values of the dimensionless charge potential z when compared to the values presented by Khrapak *et al* (2005) and Fortov *et al* (2004) [17, 28]. It should be noted, however, that both publications report errors of approximately 50% and 30%, respectively. Consequently, our results are consistent within the given uncertainties. Additionally, our results for the depleted charge potential align closely with the true values

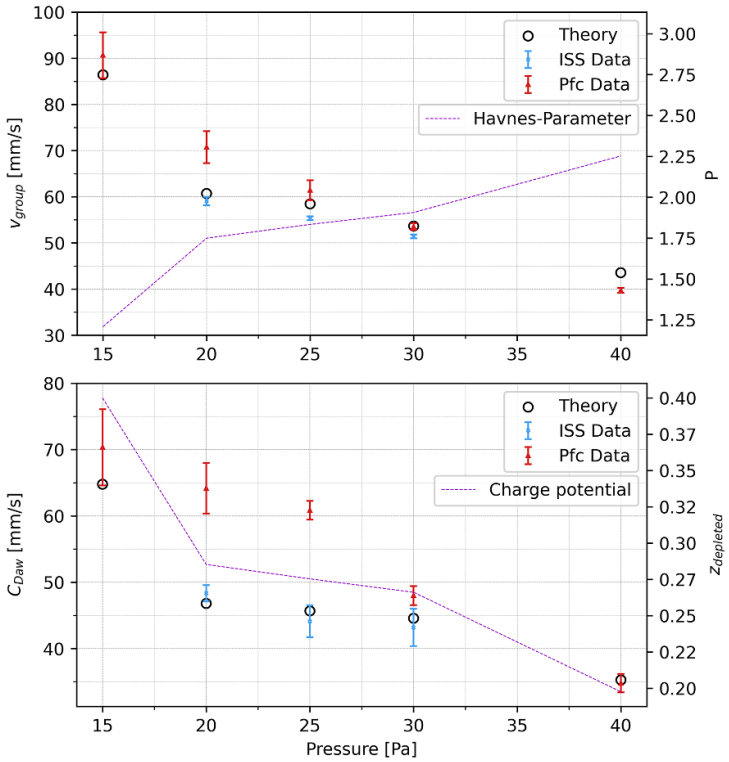


Figure 2. The figure presents the variation of group velocity v_{group} (top panel) and DAW phase velocity C_{DAW} (bottom panel) as functions of gas pressure. The data points originate from both parabolic flight (Pfc Data) and International Space Station (ISS Data) experiments, which are contrasted against theoretical predictions (denoted as 'Theory'). Additionally, the depleted charge potential z_{depleted} and the Havnes parameter P are shown to highlight the influence of large dust particle clouds on the system.

Table 2. Summary of primary performance metrics from experimental data.

Parameter	15 Pa	20 Pa	25 Pa	30 Pa	40 Pa
v_{group} $[\text{mm}\,\text{s}^{-1}]$	90.66 ± 4.98	59.06 ± 0.93	55.33 ± 0.40	51.40 ± 0.42	39.74 ± 0.53
C_{DAW} $[\text{mm}\,\text{s}^{-1}]$	70.35 ± 5.75	48.35 ± 1.24	44.11 ± 2.41	43.18 ± 2.81	34.96 ± 0.60
z	0.54 ± 0.06	0.43 ± 0.03	0.42 ± 0.02	0.41 ± 0.02	0.32 ± 0.03
z_{depl}	0.40 ± 0.06	0.29 ± 0.03	0.28 ± 0.02	0.27 ± 0.02	0.20 ± 0.03

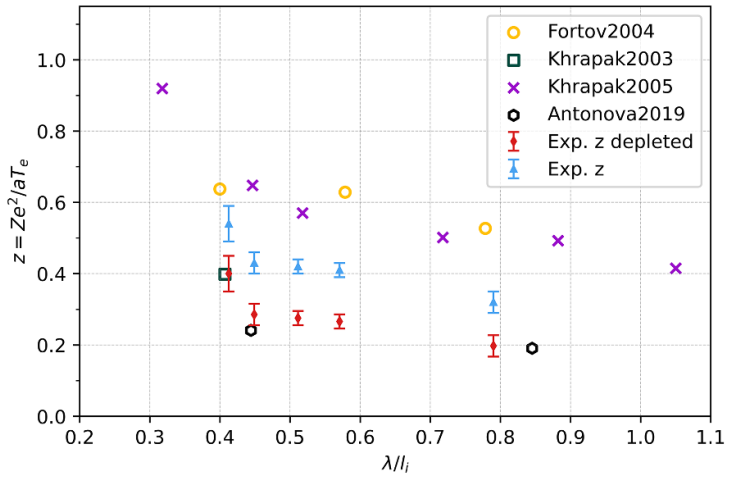


Figure 3. The charge evolution data shows variability among different studies, with experimental data points aligning with or deviating from theoretical predictions. The experimental z values, along with their reduced counterparts z_{depleted}, are illustrating these charge dynamics. The data are measured under microgravity conditions in neon with a discharge current of $I = 0.5$ mA. These results are based on multiple events, supporting significant statistical relevance.

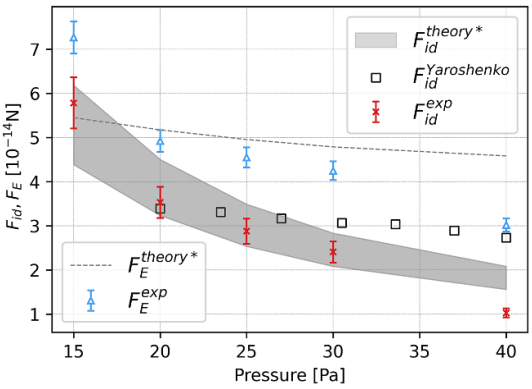


Figure 4. This figure compares the experimental findings and theoretical model predictions for the ion-drag force (F_{id}) acting on microparticles in a low-pressure plasma environment. Our experimental data are closely aligned with those published by Yaroshenko *et al* [30] and the theoretical predictions denoted as *theory**. It should be noted that the theoretical model assumes no charge depletion, highlighting its impact on the electric forces and ion-drag force.

reported by Khrapak *et al* (2003) [29] and with data from Antonova *et al* (2019) [13]. It is important to note that depletion effects were not considered in Antonova's work, likely due to the negligible particle density in those experiments.

It is important to note that the data reported herein, gathered during the ISS campaign, are derived from a comprehensive statistical database, rather than a single measurement event. The findings have been systematically and statistically analyzed across 14 experimental runs, with a total of ≈6000 frames extracted and evaluated. In contrast, the PFC data are based on a singular event for each data point measurement with ≈300 frames.

Finally, we can numerically compare the ion-drag force with previously reported results. Yaroshenko *et al* presented a method to estimate the ion-drag force without directly estimating the charge of a microparticle, using a mathematical trick involving the charge-gradient of two different microparticle sizes [30]. However, with our analytical method and improved measurements of the plasma environment through important diagnostic papers [10], we are able to make a direct comparison.

Our findings are consistent with the absolute values of the ion-drag force reported by Yaroshenko, as illustrated in figure 4. Although the previous study by Yaroshenko [30] addressed deviations in charge potential associated with reduced pressure, it did not directly account for the effects of microparticle number density and charge depletion within densely populated microparticle clouds. To highlight the importance of these factors, we compare the experimentally determined values of the ion-drag force, $F_{\mathrm{id}}^{\mathrm{exp}}$ and $F_{\mathrm{id}}^{\mathrm{Yaroshenko}}$, with theoretical predictions depicted by the light grey area and dashed line in the figure. The theoretical models, $F_{\mathrm{id}}^{\mathrm{theory}^*}$ and $F_{\mathrm{E}}^{\mathrm{theory}^*}$ assume a constant microparticle charge potential of $z^{\mathrm{theory}^*} = 0.3$ and neglect charge depletion, with a microparticle density range of $n_{\mathrm{d}}^{\mathrm{theory}^*} = 1.5 \pm 0.5 \cdot 10^{11}\,\mathrm{m}^{-3}$. The model suggests that increased particle densities enhance the ion-drag force, more pronounced at low pressure. However, they do not exert a similar influence on the electric force $F_{\mathrm{E}}^{\mathrm{theory}^*}$ in the absence of charge depletion. Our analysis reveals that lower microparticle densities are necessary when modeling at pressures below 20 Pa correctly to prevent the ion-drag force from exceeding the electric force $F_{\mathrm{E}}^{\mathrm{theory}^*}$, which would result in microparticles moving against the direction of the electric field. In consequence, the experimental data demonstrate the influence of charge depletion on the electric force, with a notable increase in deviation at lower pressures and a breakdown at higher pressure levels, affecting both $F_{\mathrm{E}}^{\mathrm{exp}}$ and $F_{\mathrm{id}}^{\mathrm{exp}}$.

To support these findings, we analyzed the absolute brightness of the images across the entire data set, where the absolute brightness is directly proportional to the particle number density n_{d}. The brightness levels during the ISS campaign were relatively constant, in contrast to those during the PFC Campaign, where absolute pixel values varied by 20% between pressures of 25–40 Pa, a variation not detectable at even lower pressures.

4.2. Electro-Rheology-Effect

In the previous section, the charge potential z of an individual particle, under the current experimental conditions, was estimated and discussed. This serves as the foundation for the subsequent analysis of the measured data. As previously described, the experimental procedure involves modulating the effective electric field by periodically switching the system's polarity with a defined duty cycle. This modulation introduces an additional phenomenon termed the electro-rheology effect where micro-particle plasma

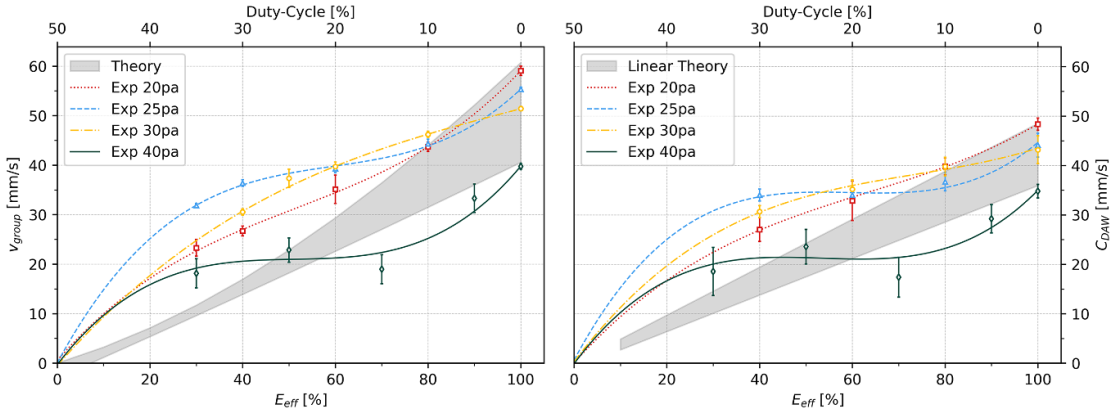


Figure 5. This figure shows the impact of the electrorheological effect on particle charge potential under varying electric field conditions. The experimental data from different pressures is fitted against a theoretical model, revealing deviations that suggest additional forces or interactions not accounted for by the model, with significant influence on DAW phase velocity.

interactions are altered. This effect modifies the potential of individual particles, influencing their interaction with both the electric field and the surrounding plasma.

This relationship is illustrated in figure 5, where the experimental data are presented in distinct colors corresponding to different pressures. A fitted curve is included to facilitate comparison with the theory, represented by the light grey region. The theory is derived from the numerical solution of the force equation (5) under the assumption of the estimated charge. The reduction of the effective electric field due to polarity switching, is modeled by adjusting the electric force (F_{E}) and the ion velocity distribution (u_{i}), calculated using the Frost formula, equation (8), contributing to the ion-drag force (F_{id}). The observed deviation of the experimental data from the theoretical prediction indicates a force or potential not accounted by the model. Notably, this deviation is also reflected in the measured DAW speeds, as these waves are determined by the Doppler shift of the collective particle cloud speed. Interestingly, the DAW velocity resembles a decelerated form of the group velocity.

To further elucidate the missing potential interaction and the differing responses of complex plasmas to DC-PS and DC fields, it is essential to consider the role of the particle potential. This potential can be modeled using a polynomial expansion that accounts for subthermal ion drift, with Mach number $M \lesssim 1$. A commonly used solution is given by equation (13). In this model, we focus on the quadrupole term, as this effect is specifically induced by the alternating current field. To estimate the behavior of the charge potential as a function of the duty cycle of the applied DC-PS field, we use the following model:

$$f_Q(x) = c_0 \cdot \left(2 - \frac{\pi}{2}\right) \cdot \left(3 \cdot \left(ax^3 + bx^2 + cx + d\right) - 1\right). \tag{14}$$

This function reconstructs the quadrupole term as defined by equation (13), with the input parameter x, representing the duty cycle applied. Using this model, the force balance equation (4) was solved by adjusting the particle charge according to the relationship $Z_{\mathrm{d}}^{\mathrm{new}} = Z_{\mathrm{d}} - Z_{\mathrm{d}} \cdot f_Q$. The final results are represented by the polynomial $p(x) = (ax^3 + bx^2 + cx + d)$, which approximates $\cos^2\Theta$, as illustrated in the right panel of figure 6. Here, the polynomial $p(x)$ demonstrates how the quadrupole influences the charge potential depending on the duty cycle [6, 31]. The outcomes of this adjustment, which reveal how the particle group velocity v_{group} responds to the duty cycle or variations of the effective electric field E_{eff}, are displayed in the left panel of figure 6. The plotted lines represent the updated model predictions, with constants a, b, c, and d determined through regression optimization methods. The experimental data was targeted, and the optimization was constrained to a maximum of 1000 steps to ensure computational efficiency. The scaling factor $c_0 \cdot \left(2 - \frac{\pi}{2}\right)$ is included to account for specific quadrupole influences.

A significant improvement in the model's predictive accuracy is observed in the left-hand panel, particularly between 20% and 60% of the effective electric field. This improvement showcases the interplay of the quadrupole effect, with the surounding plasma. Generally we find the predicted reduction of the potential, resulting in an increase of the micro particle speed v_{group}. Notable similarities are observed in the trend of our model compared to those reported by Kana *et al* [31].

Figure 6 further demonstrates how the DC-PS mode affects the particle charge potential, influencing the likelihood of particle string formation. We observe a reduction in the potential across a wide range of effective electric fields, consistent with the expected quadratic dependence of the quadrupole potential on the thermal Mach number, $\Phi_Q \propto M^2$.

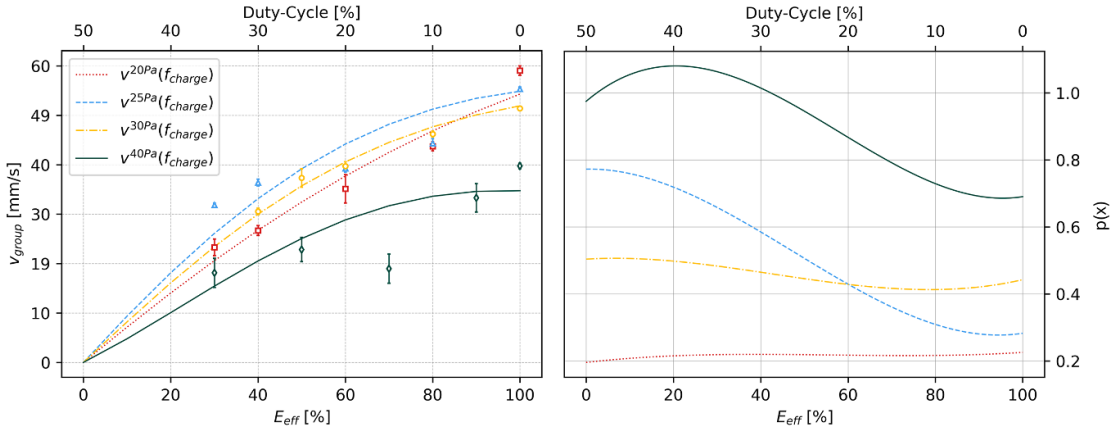


Figure 6. This figure illustrates the effects of direct current polarity switching (DC-PS) fields on particle dynamics and interactions, which lead to changes in the dust drift velocity, v_{group}, shown in the left panel, and alterations in individual particle charge through the function f_Q. The right panel displays the polynomial $p(x)$ of the model, which adjusts theoretical predictions to align with experimental data points. It represents the probability of interaction between neighboring particles, serving as a measure of electrorheological interactions [31].

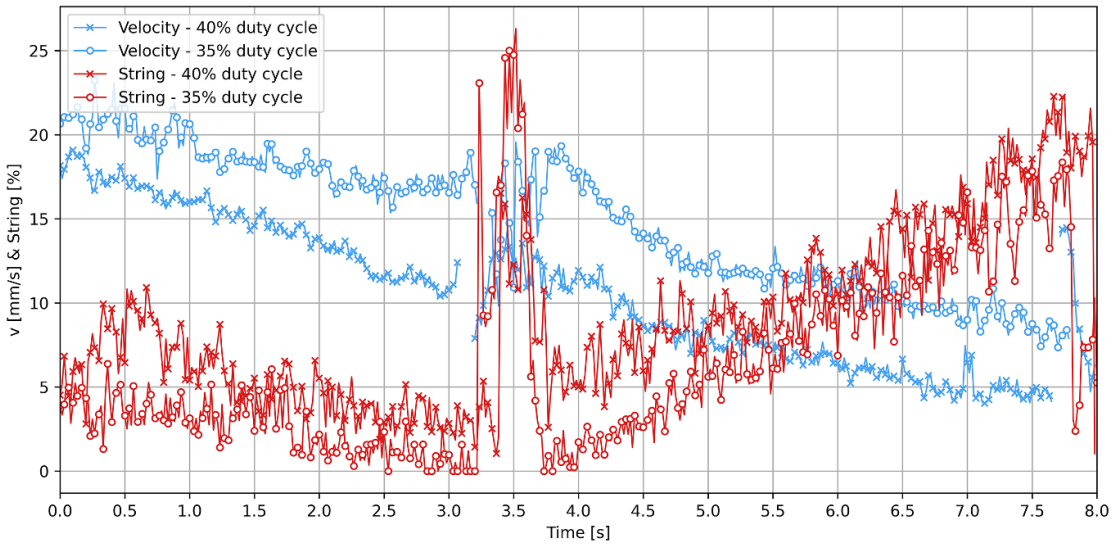


Figure 7. Velocity and string formation as a function of image number under two different duty cycles (40% and 35%) at 20 Pascal. The blue curves represent the velocity (in mm s^{-1}), while the red curves indicate the string formation percentage measured [24]. Crosses denote the 40% duty cycle, and circles indicate the 35% duty cycle for both velocity and string formation.

4.3. String formation

Polarity switching modulates the charge potential, affecting the interactions between microparticles and their surrounding environment. This modulation increases the likelihood of string formation, as reported in previous studies [8, 23], while also influencing the interaction with counteracting ions. Figure 7 illustrates a unique phenomenon observed during the ISS campaign, where a drifting microparticle cloud was exposed to a low effective electric field, revealing the impact of string formation on individual particle velocities and potentials. The observations were conducted at a pressure of 20 Pa, with two distinct duty cycles of 40% and 35%, corresponding to effective electric fields of 20% and 30%, respectively. The images were analyzed using a specialized code for particle tracing and string detection, enhanced by machine learning methods [24, 32].

An amplification in the signal is observed in the central region of the graph, corresponding to the polarity reversal of the electric field. This reversal not only induced a change in the direction of microparticle motion but also altered the charge distribution of the surrounding individual microparticles. Following the polarity switch, a distinct onset of string formation was observed, serving as a seed for crystal growth. In consequence, a notable increase in string formation was observed alongside a reduction in particle velocity, likely triggered by the reversal of the electric field potential.

During the ISS campaign, we observed a consistent discrepancy between the measured microparticle velocity and the wave phase speed, which showed an approximate increase of +15% at 20 Pa across different

polarities. This difference is most likely attributable to variations in electric field strength ($dE^{\pm} \sim 5\%$). Based on this observation, we expected an increase in measured velocity after the polarity switch. However, this was followed by a notable reduction in microparticle velocity, v. This reduction suggests that the additional energy added to the charge potential, which exceeded the interaction distance of the particles, likely facilitated the formation of strings. This formation disrupted the usual behavior of the particles, resulting in a decrease in their velocity [7, 33].

The phenomenon described involves the coupling of microparticles, indicating a transition from a liquid-like to a solid-like state in complex plasma. A comparison of the interaction radius of a microparticle, λ_D, with the interparticle distance, $(\Delta = n_d^{-1/3})$, reveals that the potential extends due to the higher electric field, such that $(2 \cdot \lambda_D/\Delta \rightarrow 1)$. The particle density was measured as constant throughout the entire data set, with $(n_d = 2 \pm 0.1 \cdot 10^{11}\,\mathrm{m}^{-3})$, using image reconstruction techniques [24]. The system then progressively consumes energy during string formation, ultimately leading to a chaotic state, characterized by the excitation of DAWs at the boundary region.

The presence of strings is expected to not only reduce the microparticle speed but also influence the phase velocity of the excited DAWs [7]. Quantitative analysis indicates that $C_{DAW}(40\%\,duty\,cycle) = 17.0 \pm 1.5\,\mathrm{mm\,s}^{-1}$, which aligns with predictions for a pressure of 20 Pa, as shown in the left panel of figure 6 and assuming a negligible Doppler shift at low effective electric field strengths. Although the electric field strength increases following the polarity switch, this does not significantly alter the DAW phase velocity, C_{DAW}. However, given the low effective Mach number, $M_{eff} = 0.3$, a slight reduction in C_{DAW} is acceptable. It is probable that the increased electric field and ER effects counteract each other, leading to the observed outcome. For the first time, a phase transition was observed in a particle cloud moving at a constant velocity, demonstrating a measurable ER effect that induced string formation.

5. Conclusion

The experimental results demonstrate that particle charge and ER effects are critical factors influencing the dynamics of microparticles in low-pressure complex plasmas under microgravity conditions. First, the charge potential, $z = 0.34 \pm 0.17$, was experimentally estimated and compared with values reported in previous studies, revealing discrepancies due to electron depletion in systems with high microparticle populations. Additionally, an increase in the charge potential to $z = 0.54 \pm 0.12$ was observed at pressures below $p \lesssim 15\,Pa$. Furthermore, we identified qualitative evidence that the potential of a microparticle is perturbed and reduced under reduced duty cycle and DC-discharge plasma conditions.

Our findings further contribute to understanding the influence of external electric fields and particle interactions on plasma wave propagation. We directly observed stepwise string formation within a particle cloud moving at a constant velocity, which affects and decelerates the multiparticle system.

Data availability statement

The data that support the findings of this study will be openly available following an embargo at the following URL/DOI: https://github.com/luki58/PFC42.

Acknowledgments

This work was supported by DLR under Grant Nos. 50WM2044 and 50WK2270B.

The work in scope of this paper of A V Z, A M L, A D U and O F P was also supported by the Ministry of Science and Higher Education of the Russian Federation (State Assignment No. 075-00269-25-00).

All authors greatly acknowledge the joint ESA-Roscosmos 'Experiment Plasmakristall-4' onboard the ISS. We also express our gratitude to Mikhail Pustylnik and Hubertus Thomas from DLR for their support, as well as to CAMDMOS for their assistance during the ISS campaigns.

ORCID iDs

L Wimmer https://orcid.org/0009-0008-8970-8203
M Klein https://orcid.org/0009-0009-9596-7671
A M Lipaev https://orcid.org/0000-0002-2559-3696

References

[1] Zohm H 2012 Plasmaphysik *Technical Report* (Ludwig-Maximilian-University Munich) (available at: www.ipp.mpg.de/2155286/Plasmaphysik)
[2] Merlino R 2009 Dust-acoustic waves driven by an ion-dust streaming instability in laboratory discharge dusty plasma experiments *Phys. Plasmas* **16** 124501
[3] Schwabe M *et al* 2008 Nonlinear waves externally excited in a complex plasma under microgravity conditions *New J. Phys.* **10** 033037
[4] Merlino R L 2014 25 years of dust acoustic waves *J. Plasma Phys.* **80** 773–86
[5] Fortov V E, Khrapak A G, Khrapak S A, Molotkov V I, Nefedov A P, Petrov O F and Torchinsky V M 2000 Mechanism of dust-acoustic instability in a direct current glow discharge plasma *Phys. Plasmas* **7** 1374–80
[6] Dietz C, Budak J, Kamprich T, Kretschmer M and Thoma M H 2021 Phase transition in electrorheological plasmas *Contrib. Plasma Phys.* **61** e202100079
[7] Schwabe M *et al* 2020 Slowing of acoustic waves in electrorheological and string-fluid complex plasmas *New J. Phys.* **22** 083079
[8] Ivlev A V, Thoma M H, Räth C, Joyce G and Morfill G E 2011 Complex plasmas in external fields: the role of non-hamiltonian interactions *Phys. Rev. Lett.* **106** 155001
[9] Dietz C, Kretschmer M, Steinmüller B and Thoma M 2018 Recent microgravity experiments with complex direct current plasmas *Contrib. Plasma Phys.* **58** 21–29
[10] Pustylnik M Y *et al* 2016 Plasmakristall-4: new complex (dusty) plasma laboratory on board the International Space Station *Rev. Sci. Instrum.* **87** 093505
[11] Thoma M H *et al* 2010 Recent complex plasma experiments in a dc discharge *IEEE Trans. Plasma Sci.* **38** 857–60
[12] Kretschmer M, Antonova T, Zhdanov S and Thoma M 2015 Wave phenomena in a stratified complex plasma *IEEE Trans. Plasma Sci.* **44** 458–62
[13] Antonova T, Khrapak S A, Pustylnik M Y, Rubin-Zuzic M, Thomas H M, Lipaev A M, Usachev A D, Molotkov V I and Thoma M H 2019 Particle charge in PK-4 dc discharge from ground-based and microgravity experiments *Phys. Plasmas* **26** 113703
[14] Fortov V, Ivlev A, Khrapak S, Khrapak A and Morfill G 2005 Complex (dusty) plasmas: current status, open issues, perspectives *Phys. Rep.* **421** 1–103
[15] Melzer A 2019 *Physics of Dusty Plasmas* (Springer Cham)
[16] Zobnin A V, Usachev A D, Petrov O F and Fortov V E 2008 Ion current on a small spherical attractive probe in a weakly ionized plasma with ion-neutral collisions (kinetic approach) *Phys. Plasmas* **15** 043705
[17] Khrapak S A *et al* 2005 Particle charge in the bulk of gas discharges *Phys. Rev.* E **72** 016406
[18] Khrapak S A, Ivlev A V, Morfill G E and Thomas H M 2002 Ion drag force in complex plasmas *Phys. Rev.* E **66** 046414
[19] Liu B, Goree J, Nosenko V and Boufendi L 2002 Radiation pressure and gas drag forces on a melamine-formaldehyde microsphere in a dusty plasma *Phys. Plasmas* **10** 9–20
[20] Khrapak S A and Khrapak A G 2019 Modified Frost formula for the mobilities of positive ions in their parent gases *AIP Adv.* **9** 095008
[21] Fortov V E, Usachev A D, Zobnin A V, Molotkov V I and Petrov O F 2003 Dust-acoustic wave instability at the diffuse edge of radio frequency inductive low-pressure gas discharge plasma *Phys. Plasmas* **10** 1199–208
[22] Wimmer L, Schmitz A S, Kretschmer M and Thoma M H 2024 Tilted dust-acoustic waves in low-pressure DC complex plasma *Phys. Plasmas* **31** 043702
[23] Mitic S *et al* 2021 Long-term evolution of the three-dimensional structure of string-fluid complex plasmas in the pk-4 experiment *Phys. Rev.* E **103** 063212
[24] Klein M, Dormagen N, Dietz C, Thoma M and Schwarz M 2024 Enhancing particle string detection in electrorheological plasmas using asymmetrical kernel convolutional networks *Mach. Learn.: Sci. Technol.* **5** 025050
[25] Dormagen N, Klein M, Schmitz A S, Thoma M and Schwarz M 2024 Multi-particle tracking in complex plasmas using a simplified and compact u-net *J. Imaging* **10** 40
[26] Nosenko V *et al* 2020 Shear flow in a three-dimensional complex plasma in microgravity conditions *Phys. Rev. Res.* **2** 033404
[27] Liu B, Goree J and Suranga Ruhunusiri W D 2015 Characterization of three-dimensional structure using images *Rev. Sci. Instrum.* **86** 033703
[28] Fortov V E, Petrov O F, Usachev A D and Zobnin A V 2004 Micron-sized particle-charge measurements in an inductive rf gas-discharge plasma using gravity-driven probe grains *Phys. Rev.* E **70** 046415
[29] Khrapak S *et al* 2003 Compressional waves in complex (dusty) plasmas under microgravity conditions *Phys. Plasmas* **10** 1–4
[30] Yaroshenko V *et al* 2005 Determination of the ion-drag force in a complex plasma *Phys. Plasmas* **12** 093503
[31] Kana D, Dietz C and Thoma M H 2020 Simulation of electrorheological plasmas with superthermal ion drift *Phys. Plasmas* **27** 103703
[32] Klein M, Dormagen N, Schmitz A S, Thoma M H and Schwarz M 2023 Machine learning approach for particle matching, tracing and velocimetry with self-organizing map: application to complex plasmas *2023 Int. Conf. on Machine Learning and Applications (ICMLA)* (IEEE) pp 839–44
[33] Rosenberg M 2015 Waves in a 1d electrorheological dusty plasma lattice *J. Plasma Phys.* **81** 905810407